ICSO 2016

International Conference on Space Optics

Biarritz, France

18–21 October 2016

Edited by Bruno Cugny, Nikos Karafolas and Zoran Sodnik

Wave front sensing for next generation earth observation telescope

J.-M. Delvit

C. Thiebaut

C. Latry

G. Blanchet

esa icso proceedings cnes

International Conference on Space Optics — ICSO 2016, edited by Bruno Cugny, Nikos Karafolas, Zoran Sodnik, Proc. of SPIE Vol. 10562, 105625H · © 2016 ESA and CNES
CCC code: 0277-786X/17/$18 · doi: 10.1117/12.2296162

WAVE FRONT SENSING FOR NEXT GENERATION EARTH OBSERVATION TELESCOPE

J.-M. Delvit[1], C. Thiebaut[1], C. Latry[1], G. Blanchet[1]
[1] *Centre National d'Etudes Spatiales (CNES), 18 av. Edouard Belin, 31401 Toulouse, France*

INTRODUCTION

High resolution observations systems are highly dependent on optics quality and are usually designed to be nearly diffraction limited. Such a performance allows to set a Nyquist frequency closer to the cut off frequency, or equivalently to minimize the pupil diameter for a given ground sampling distance target. Up to now, defocus is the only aberration that is allowed to evolve slowly and that may be inflight corrected, using an open loop correction based upon ground estimation and refocusing command upload. For instance, Pleiades satellites defocus is assessed from star acquisitions and refocusing is done with a thermal actuation of the M2 mirror. Next generation systems under study at CNES should include active optics in order to allow evolving aberrations not only limited to defocus, due for instance to in orbit thermal variable conditions. Active optics relies on aberration estimations through an onboard Wave Front Sensor (WFS). One option is using a Shack Hartmann. The Shack-Hartmann wave-front sensor could be used on extended scenes (unknown landscapes). A wave-front computation algorithm should then be implemented on-board the satellite to provide the control loop wave-front error measure. In the worst case scenario, this measure should be computed before each image acquisition. A robust and fast shift estimation algorithm between Shack-Hartmann images is then needed to fulfill this last requirement. A fast gradient-based algorithm using optical flows with a Lucas-Kanade method has been studied and implemented on an electronic device developed by CNES.
Measurement accuracy depends on the Wave Front Error (WFE), the landscape frequency content, the number of searched aberrations, the a priori knowledge of high order aberrations and the characteristics of the sensor.
CNES has realized a full scale sensitivity analysis on the whole parameter set with our internally developed algorithm. The aim of this paper is to present a synthesis of this benchmark and will address the following points:
- Introduction of the context of active optics for high resolution Earth remote sensing
- Principles of Shack Hartmann wave front sensor
- Brief presentation of CNES solving algorithm
- Main results

I. OPTICAL HYPOTHESIS

A. Optical requirements

The telescope characteristics are determined by the angular resolution goal, the image sensor parameters and the image requirements. The camera concept is a push-broom system. The mission [8] consists in covering a +/-0.61° field of view with 30cm ground pixels. The satellite altitude is 700 km. The angular resolution is 0.43 µrad. Alternative image sensors have been studied. In particular a two-dimensional array associated with a fast telescope (F-number from 5.4 to 8.5) can be an interesting solution. In this paper we only take into account a classical Korsch design. The optical modulation transfer function (MTF) requirement is to guarantee a 0.25 optical MTF at frequency corresponding to 30 cm on ground.

B. Optical design

A comparative study has been led at CNES. Several compact optical designs (TMA, catadioptric and Korsch concepts) with different apertures, from F/5.4 to F/20, have been studied and compared [7]. For long focal length telescopes, the Korsch concept is the most common and is chosen for its compactness and for several optical key advantages: it allows an easy design of a diffraction limited system, little occultation, easy baffling thanks to an intermediate image and a real exit pupil.

The axial dimension is more than eleven times smaller than the focal length. The fore optics (primary and secondary mirrors) is the very sensitive part. The aft part, kept behind the primary mirror, is much more tolerant. Table 1 gives the main characteristics of our optical design.

Optical characteristic	Korsch F/20 design
Telescope Focal length	30 m
Primary mirror f-number	1.5
Secondary mirror f-number	1.8
Tertiary mirror f-number	5.8
Axial Primary mirror magnification	165
Axial Secondary mirror magnification	170
Axial Tertiary mirror magnification	6.5

Table 1. Optical main characteristics of Korsch design

C. Optical performances

The optical MTF requirement is 0.25 at the frequency of interest. Its value of 1.17 10^6 rad^{-1} corresponds to an instantaneous field of view of 30 cm at 700 km altitude. The opto-mechanical sensitive terms are the focus, the decentering and the tilt amplitude of the fore optics. Table 2 gives the budget corresponding to an optical MTF of 0.25. The optical distortion is also an important performance regarding the use of a time delay and integration sensor. These opto-mechanical tolerances are challenging [8]. The optical distortion is acceptable.

Optical performance	Korsch F/20
Optical Theoretical MTF	0.34
Focus tolerance	1.35 µm
Decentering tolerance	13.5 µm
Tilt tolerance	13.5 µrad
X distorsion	0.9 %
Y distorsion	0.3 %

Table 2. Main optical performances

II. ACTIVE OPTICS PRINCIPLES

Two types of defaults contribute to the wave front error degradation: alignment and shape errors of the optics.

In the Korsch telescope (figure 1), a positioning mechanism is implemented behind the secondary mirror in order to compensate total or partial alignment defaults of the fore optics. The first step of this approach is very well known: it consists in adjusting the focus term of the optical system. The challenge is now to generalize this compensation to alignment aberrations. This mechanism is implemented in the fore optics, because it is the most sensitive part. It can be a 3 or 5-degree of freedom mechanism depending on the performance capacities of the mechanism and depending on the WFE performance objectives. This approach enables us to cope with the stringent opto-mechanical requirements. A deformable mirror is implemented at the pupil stop in order to compensate mirror shape errors. The deformable mirror is in the aft part thanks to the real Korsch exit pupil. This approach enables us to simplify the primary mirror requirements. The assessment of the wave front error is done by a wave front sensor. CNES has studied two kinds of WFS: a WFS based on phase diversity algorithm [9], and a WFS based on a Shack Hartman [2], [6]. This paper describes a Shack Hartmann for Earth observation working on extended landscape.

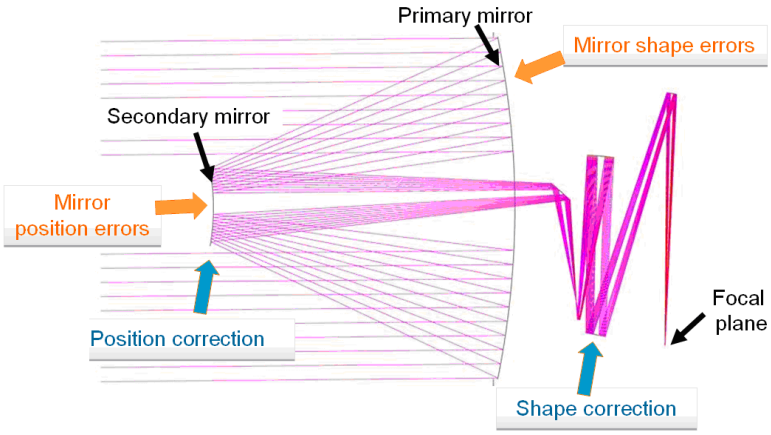

Figure 1 - Active optics principle

III. FAST GRADIENT-BASED ALGORITHM FOR SHIFT COMPUTATION BETWEEN SHACK-HARTMANN IMAGES

A Shack-Hartmann wavefront sensor is an instrument used to compute the error between the real wavefront error (with aberrations) and the perfect one (without aberrations) defined as below:

$$WFE(i,j)= \varphi_{i,j} \times \lambda_{eq}/2\pi$$

with $\varphi_{i,j}$ the phase differential in each point of the pupil and λ_{eq} the central wavelength of the considered spectral band, here 650 nm.

The Shack-Hartmann is composed with a lenslets array and a 2D detector array in the focal plane. Each lenslet generates on the sensor an impulse (in a point source mode) or an image (in an extended source mode) whose position varies according to the local wavefront error. The reference position corresponds to a perfect wavefront obtained without any optical aberrations. The deviation of each spot (in the point source mode) compared to the reference position gives the local slope of the wavefront, the whole slopes giving the wavefront's gradient. Well-known algorithms allow going back to the wavefront from computed slopes [4]. To do this estimation correctly on extended scenes, the Shack-Hartmann sensor should be carefully dimensioned. It is possible to adapt both the collimator's diameter and focal length, the number of lenslets and their focal length and size and the size of the 2D detector array. For the planned Earth observation missions, typical Shack-Hartmann sizing will lead to lenslets of size around 40x40 pixels. An example of WFE and the associated lenslets is shown Figure 2.

Furthermore, optical combination generally leads to an occultation mask with a hole in the center and in the region of the arms. In these areas, lenslets have less signal (occulted signal) and the MTF of each images are different. It is then possible to keep or reject these lenslets in the wavefront computation from the slopes as shown Figure 3. The percentage of non-occultation is a parameter of the algorithm. The less lenslets we keep, the faster the algorithm will be, but the wavefront reconstruction needs enough lenslets to be fair.

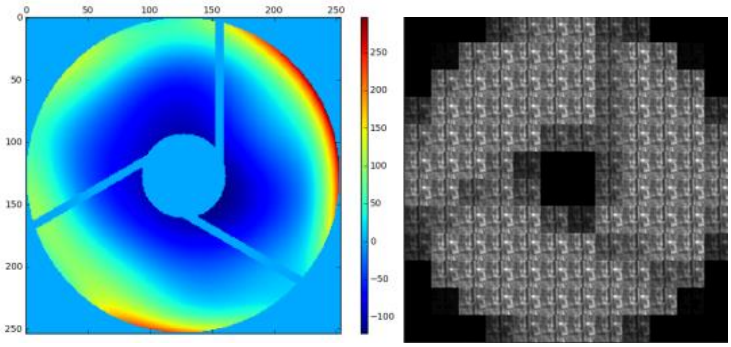

Figure 2 - Left – example of a WFE with only low-orders Zernike polynomials. Right – lenslets associated with the WFE from the left figure on an extended landscape. Lenslets with lower signal can be seen around the center and the arms.

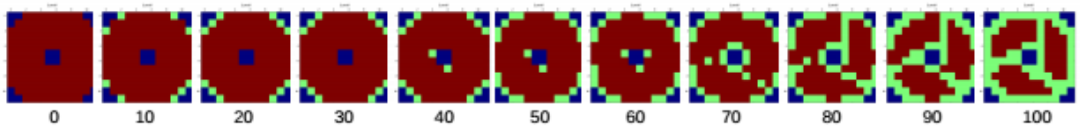

Figure 3 – From left to right – illustration of the non-occultation percentage, slopes of lenslets in red are used to compute the wavefront error. The ones in green are rejected.

To compute shifts between all lenslets and a reference one, we have selected an algorithm based on optical flow with Lucas-Kanade solving [3],[6],[10]. This method has been selected for its low complexity. Optical flow method tends to link difference between two consecutives images (in terms of temporal evolution) with the gradient of the spatial intensity of the first one. Note $I_1(x,y)$ and $I_2(x,y)$ two images to correlate, v_x and v_y translations in x and y between I_1 and I_2 :

$$I_2(x,y) \approx I_1(x - v_x, y - v_y) \tag{1}$$

Under the hypothesis of small translations values and using Taylor's theorem, we obtain:

$$I_2(x,y) \approx I_1(x,y) - v_x \frac{\partial I_1(x,y)}{\partial x} - v_y \frac{\partial I_1(x,y)}{\partial y} \tag{2}$$

Then

$$I_t(x,y) = I_1(x,y) - I_2(x,y) \approx v_x \frac{\partial I_1(x,y)}{\partial x} + v_y \frac{\partial I_1(x,y)}{\partial y} \tag{3}$$

Meaning $I_t(x,y) \cong \nabla I_1(x,y)v$ with $\nabla I_1(x,y) = \left[\frac{\partial I_1(x,y)}{\partial x}, \frac{\partial I_1(x,y)}{\partial y}\right]$, $v = \begin{bmatrix} v_x \\ v_y \end{bmatrix}$

A solution of this problem has been proposed by Lucas-Kanade [3] under the hypothesis that the shift v is the same for all pixels of images I_1 and I_2. This leads to the over-determined problem Av=b with:

$$A = \begin{pmatrix} \frac{\partial I_1}{\partial x}(p_1) & \frac{\partial I_1}{\partial y}(p_1) \\ \vdots & \vdots \\ \frac{\partial I_1}{\partial x}(p_n) & \frac{\partial I_1}{\partial y}(p_n) \end{pmatrix}, v = \begin{bmatrix} v_x \\ v_y \end{bmatrix}, b = -\begin{pmatrix} \frac{\partial I_1}{\partial t}(p_1) \\ \vdots \\ \frac{\partial I_1}{\partial t}(p_n) \end{pmatrix}$$

With p^i i^{th} pixel of the image and n number of pixels if I_1. This system is solved by a least-squares method: $A^TA\,v = A^Tb$

$$A^TA = \begin{bmatrix} \sum {I_x}^2 & \sum I_x I_y \\ \sum I_x I_y & \sum {I_y}^2 \end{bmatrix} \text{ and } A^Tb = \begin{bmatrix} \sum I_t I_x \\ \sum I_t I_y \end{bmatrix}$$

$$\text{With } I_x = \frac{\partial I_1}{\partial x},\ I_y = \frac{\partial I_1}{\partial y},\ I_t = \frac{\partial I_1}{\partial t} = I_2 - I_1$$

If A^TA is invertible, the solution is $(A^TA)^{-1}A^Tb$.

$$\widehat{v_x} = \frac{1}{\text{Det}}\left(\sum I_t I_x \sum {I_y}^2 - \sum I_t I_y \sum I_y I_x\right) \tag{4}$$

$$\widehat{v_y} = \frac{1}{\text{Det}}\left(\sum I_t I_y \sum {I_x}^2 - \sum I_t I_x \sum I_y I_x\right) \tag{5}$$

$$\text{With Det} = \sum {I_y}^2 \sum {I_x}^2 - \left(\sum I_x I_y\right)^2$$

The translation values can then be computed thanks to the gradient of the first image in both vertical and horizontal directions and to the difference between the two images (Equations 4 and 5).

For the Shack-Hartmann, we only consider a translation in both directions between lenslets and no more than a translation. The value of the translation is quite small because the wavefront error we plan to measure and control is associated with shifts lower than tenth a pixel. The reference lenslet chosen for shift computation is one with high signal (non-occulted). For the on-board implementation of the algorithm, the reference image is

always the same. The horizontal gradient (respectively vertical) image of this reference image is computed using the difference between a pixel and its right neighbor (respectively bottom neighbor) [5].

Because Taylor's theorem assumptions are not always true (shifts << 1) when computing shifts between two lenslets, we compute the shifts iteratively, resampling the studied images between two iterations. After this resampling, shifts between the reference and the image are lower and Taylor's assumptions are validated. The number of iterations and the filter to perform image resampling is a parameter of the algorithm. The reference software we have developed to validate the Shack-Hartmann performances is able to go up to 100 iterations with more or less complex resampling filters. For the on-board implementation, the value of the iteration number has been fixed.

Moreover, because lenslets have different signal levels (occultation mask), it is needed to homogenize them radiometrically taking into account the area of occultation for each of them.

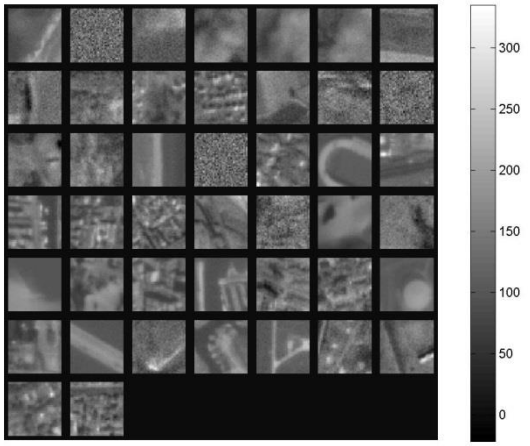

Figure 4– the 44 landscapes used for the validation - 44 landscapes taken from PLEIADES images have been used to simulate Shack-Hartmann images with representative wavefront errors and wavefront sensor.

This algorithm has been validated on different landscapes: 44 landscapes taken from PLEIADES images [1] have been used to simulate Shack-Hartmann images with representative wavefront errors and wavefront sensor sizing. The Figure 4 presents the 44 landscapes that have been used for validation (numbered 1 to 44 from the upper left hand side to the bottom right hand side). Some of these landscapes contain only noise, some of them are cloudy to be representative of different scenes the wavefront sensor could have to deal with. The figure 5 shows the results obtained with the proposed algorithm described above for each of the 44 landscapes with the wavefront error presented in Figure 2. The error is an RMS error between the real wavefront error and the estimated one with a reconstruction of the WFE through a Zernike polynomials from the estimated shifts between lenslets. For most of the 44 landscapes, RMS error is lower than 20nm and more than 60% is under 10nm which is very efficient. These performances have been computed with 100 possible iterations of the optical flows. All this analysis has been confirmed by simulations on several WFE, with or without high frequency, with different high frequency shapes, with different amplitudes…

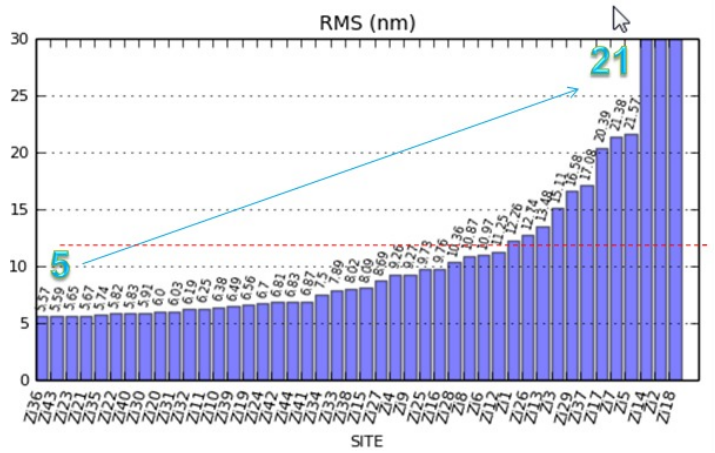

Figure 5 – the results obtained with the proposed algorithm described for each of the 44 landscapes (figure 5) with the wavefront error presented in Figure 2.

IV. IMPLEMENTATION OF THE SHACK-HARTMANN FAST GRADIENT-BASED ALGORITHM

The implemented version of the algorithm [10] uses only two iterations and gives results comparable to the reference software in terms of wave-front error assessment (see Figure 6).

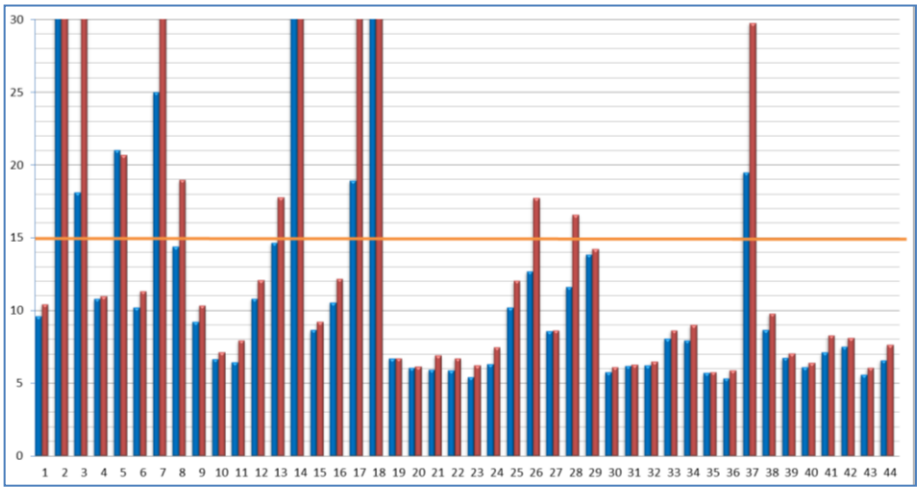

Figure 6 – Wavefront error reconstruction between the reference algorithm (in blue) and the implemented one with only two iterations of the optical flows (in red). X axis is the landscape number; Y axis is the wavefront error reconstruction in RMS for wavefront presented in Figure 2.

The implemented version of the algorithm on the CPUgen described in [10] computes a shift between two lenslets of around 40 pixels in 1.5ms at 20 MHz. Finally, for a Shack-Hartmann sensor with 100 lenslets, the total computation time of the shifts will be 150ms for an iteration and thus around 300ms for two iterations.
With this implementation, it is possible to measure the WFE on 3 different landscapes in less than one second.

VI. CONCLUSION

Next generation systems under study at CNES should include active optics in order to allow evolving aberrations not only limited to defocus, due for instance to in orbit thermal variable conditions. Active optics clearly improves the quality of the images produced by this kind of telescope reaching the diffraction limit. Such a performance allows setting a Nyquist frequency closer to the cut off frequency, minimizing the pupil diameter for a given ground sampling distance target.
The Shack-Hartmann wave-front sensor can be used on extended scenes and unknown landscapes to assess the WFE. The wave-front computation algorithm proposed can be implemented on-board the satellite to provide the control loop wave-front error measure. In the worst case scenario, this measure is computed before each image acquisition. A robust and fast shift estimation algorithm between Shack-Hartmann images is then needed to fulfill this last requirement. The fast gradient-based algorithm using optical flows presented in this paper is very accurate and very fast. It allows processing 3 images in one second with accuracy better than 20nm. Some

landscapes are disadvantageous for shift estimation because of low signal to noise ratio or because of a main direction in the image (road, coasts…). Selection of favorable landscapes opposed to bad ones can be performed with selection criteria computed during the optical flow (Cramer-Rao Lower Bound and eigenvalues of the Fisher Information Matrix).
A first representative validation of the performance closed loop is expected in 2017. This validation will include a qualified deformable mirror and representative metrology. A full scale demonstrator of an active telescope is expected for 2018.

REFERENCES

[1] A. Gleyzes et al., "Pleiades system architecture and main performances", proceedings of ISPRS, Melbourne, 2012
[2] B. C. Platt & R. Shack, "History and Principles of Shack-Hartmann Wavefront Sensing", in Journal of Refractive Surgery Volume 17, 2001
[3] B. D. Lucas and T. Kanade, "An iterative image registration technique with an application to stereo vision," in Proc. of the 7th Int. Joint Conf. on Artificial intelligence - Volume 2, ser.IJCAI'81. San Francisco, CA, USA, 1981.
[4] R. J. Noll, "Phase estimates from slope-type wavefront sensors," J. Opt. Soc. Am.68, 1978
[5] M. Rais et al., "A tight multiframe registration problem with application to Earth observation satellite design", in Proc. of IEEE Int. Conf. on Imaging Systems and Techniques, Santorin, Grèce, 2014.
[6] A. Bonnefois et al. 2014 Comparative theoretical and experimental study of a Shack-Hartmann and a Phase Diversity Sensor, for high-precision wavefront sensing dedicated to Space Active Optics ICSO 2014.
[7] V. Costes et al. , "Optical design and adaptive optics for next generation space telescope." SPIE, UV/Optical/IR Space Telescopes and Instruments: Innovative Technologies and Concepts VI, volume 8860, 2013.
[8] V. Costes et al., "Active optics for next generation space telescopes", ICSO, Biarritz, 2016
[9] C. Latry et al., "Sensitivity analysis of phase diversity technique for high resolution earth observing telescopes", ICSO, Biarritz, 2016
[10] C. Thiebaut et al. "Fast gradient-based algorithm on extended landscapes for wave-front reconstruction of Earth observation satellite", proceedings of SPIE Astronomical Telescope, 2016